Available online at www.sciencedirect.com
ScienceDirect
Trans. Nonferrous Met. Soc. China 32(2022) 850−867
Transactions of Nonferrous Metals Society of China
www.tnmsc.cn

Quantitative analysis of globularization and modeling of TC17 alloy with basketweave microstructure

Hao-yu PANG, Jiao LUO, Zhi-gang ZHANG, Wen-chao HAN, Keng-feng XU, Miao-quan LI

State Key Laboratory of Solidification Processing, Northwestern Polytechnical University, Xi'an 710072, China

Received 31 March 2021; accepted 20 November 2021

Abstract: The globularization behavior and mechanism of TC17 alloy with basketweave microstructure were investigated, and the models of dynamic and static globularization kinetics were established. The quantitative and metallographic results show that the globularization of α phase is sensitive to the parameters of deformation and heat treatment. By EBSD analysis, the formation and evolution mechanisms of intra-α boundaries are related to discontinuous dynamic recrystallization and continuous dynamic recrystallization, which can form α grains with high and low misorientations between neighbour grains after the heat treatment, respectively. Based on the globularization behavior and mechanism, two modified JMAK models are developed to predict the dynamic and static globularization kinetics, and the mean absolute relative errors (MARE) of 10.67% and 13.80% indicate the accuracy of the dynamic and static globularization kinetics models. The results of this work can provide guidance for controlling microstructure of titanium alloy.

Key words: TC17 alloy; basketweave microstructure; globularization; quantitative analysis; kinetics model

1 Introduction

TC17 alloy, a near β titanium two-phase alloy, has been widely used to manufacture compressor disks, fan blades and blisks due to its high strength, high toughness and good hardenability [1,2]. As known, the mechanical properties of titanium alloy are closely related to microstructure [3,4]. With the development of aviation industry in recent years, aviation components with more excellent mechanical performance and more refined microstructure are required. For example, a dual-property blisk needs basketweave microstructure in disk sections and equiaxed microstructure in blades to meet the performance requirements [5−7]. As a consequence, it is of great concern to control the morphology of α phase in titanium alloy to meet the microstructure and property requirements.

It is vital to understand the effect of deformation and heat treatment parameters on the globularization behaviors of α phase in order to tailor the microstructure. Dynamic globularization kinetics of TA15 [8], TC11 [9] and BT25 [10] alloys was quantitatively analyzed, and the results showed that the globularization fraction of α phase approximately increased with increasing strain in a sigmoid way, and also increased with increasing deformation temperature and decreasing strain rate. The Avrami type equation was appropriately used to describe the dynamic globularization kinetics and the critical strain for globularization (ε_c) was obtained by fitting [8−10]. After deformation, the globularization of α lamellae can be greatly promoted by heat treatment. Therefore, the static globularization kinetics of TC11 [11], Ti−6Al−4V [12] and TA15 [13] alloys was quantitatively analyzed and the results showed that the static globularization of α lamella was accelerated with increasing pre-deformation strain and heat treatment temperature.

Corresponding author: Jiao LUO, Tel: +86-29-88460465, E-mail: luojiao@nwpu.edu.cn
DOI: 10.1016/S1003-6326(22)65838-2
1003-6326/© 2022 The Nonferrous Metals Society of China. Published by Elsevier Ltd & Science Press

XU et al [14] pointed out that the static globularization behaviors of Ti-17 alloy were similar at two pre-deformation temperatures. In addition, the static globularization kinetics could also be described by the JMAK equation due to similarity of static globularization and static recrystallization [13].

The mechanisms of microstructure evolution during globularization were also focused by many researchers. Boundary splitting was a main mechanism of globularization during deformation and heat treatment, which was accomplished with formation of intra-α boundaries and the penetration of β phase [15−17]. LI et al [18,19] indicated that high angle grain boundaries (HABs) in α lamellae were mainly induced by continuous dynamic recrystallization (CDRX) during deformation. GAO et al [20] pointed out that the main globularization mechanism of Ti−6.5Al−2Zr−1Mo−1V alloy with lamellar microstructure during hot deformation was boundary splitting, which was the result of out-of-step rotation of crystal structure in α lamellae. Besides, it was found that fine near-equiaxed particles were generated at the α/β interface of Ti−6Al−4V alloy [21,22] and TA15 alloy [23] after deformation, which indicated that discontinuous dynamic recrystallization (DDRX) occurred. LI et al [24] studied the dynamic globularization mechanisms of Ti−6.5Al−3.5Mo−1.5Zr−0.3Si alloy with lamellar microstructure by SEM and TEM techniques, and indicated that CDRX and DDRX are the dominating globularization mechanisms at strain rate of 0.01 s^{-1} and 0.1−10 s^{-1}, respectively. Nevertheless, the specific formation and evolution process of the intra-α boundaries associated with recrystallization are still unclear.

The objective of this work is to quantitatively analyze the dynamic and static globularization behaviors of TC17 alloy with basketweave microstructure and investigate the formation and evolution mechanisms of intra-α boundaries. Consequently, dynamic and static globularization kinetics models are established. For this purpose, the optical micrograph observation and quantitative analysis of TC17 alloy after deformation and heat treatment were carried out. In addition, the boundary misorientation distribution in α phase was measured using EBSD. In particular, the local crystal orientation near the intra-α boundaries was investigated in order to further understand the formation and evolution of intra-α boundaries. Then, the kinetics models were established based on the study of globularization behavior and mechanism. The present work will provide guidance for designing and controlling the microstructure of TC17 alloy.

2 Experimental

2.1 Materials

The material used in the present study was Ti−5Al−2Sn−2Zr−4Mo−4Cr, also designated as TC17 alloy. The compositions (mass fraction) of TC17 alloy used in the present work are presented in Table 1, and the β transus temperature of this alloy is approximately 905 °C [25].

Table 1 Chemical compositions of TC17 alloy used in this study (wt.%)

Ti	Al	Sn	Zr	Mo	Cr
Bal.	5.12	2.03	2.10	4.04	3.94
Fe	C	N	H	O	
0.10	0.012	0.007	0.007	0.12	

The TC17 alloy had initial basketweave microstructure, which consisted of α lamellae, intergranular α and β matrix, as shown in Fig. 1. The α lamellae interweaved well with each other, and the intergranular α distributed discontinuously at the original β grain boundaries with an average thickness of 2.55 μm.

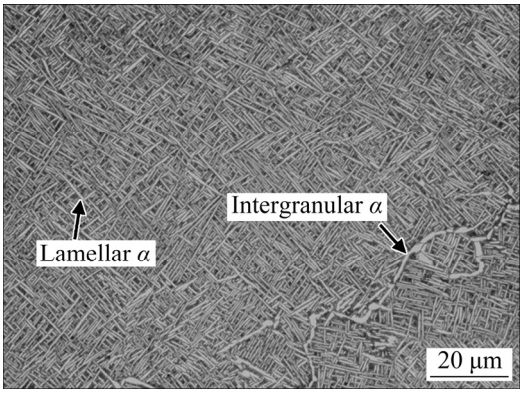

Fig. 1 Initial microstructure of TC17 alloy

2.2 Isothermal compression and heat treatment

Cylinder specimens with 12.0 mm in height and 8.0 mm in diameter were machined from the as-received TC17 bar. The specimens were heated

to deformation temperature at linear heating rate of 10 °C/s and maintained at that temperature for 5 min to ensure uniform distribution of temperature inside the specimens. Then, the specimens were isothermally compressed on a Gleeble−3500 thermal simulator at the deformation temperatures of 740, 780 and 820 °C, strain rates of 0.01, 0.1 and 1 s^{-1} and true strains of 0.22, 0.36, 0.69 and 1.20. A graphite foil was added between the specimens and anvil in order to reduce the friction. After deformation, the compressed specimens were water-quenched to preserve the deformed microstructure. Deformed specimens were annealed in a KSL−1400XA4 furnace at 720, 760 and 800 °C for 1, 2 and 4 h. After annealing, the specimens were air-cooled to room temperature.

2.3 Microstructure examination

All the deformed and heat-treated specimens were sectioned along the axis, and then mechanically ground and polished. After polishing, the specimens were etched in a solution of 10% HF, 15% HNO_3 and 75% H_2O (volume fraction) for optical microscopy (OM) analysis. The metallographs were taken from the central portion of specimens to quantitatively analyze the microstructure evolution.

Electron backscattered diffraction (EBSD) measurement was carried out to investigate the possible mechanisms for the microstructure evolution. After being axially sectioned and mechanically ground, the specimens were electropolished in a solution of 6% $HClO_4$, 30% $CH_3(CH_2)_3OH$ and 64% CH_3OH using the polishing parameters of 20 V, 16 °C and 40 s. The EBSD measurement was carried out on a Carl Zeiss Merlin Compact field emission scanning electron microscope (SEM) equipped with an Oxford Nordlys Max EBSD detector. The measurements were carried out in the central region of the specimen in an area of 35 μm × 35 μm with a step size of 0.1 μm and an acceleration voltage of 20 kV.

2.4 Quantitative analysis

The micrographs were analyzed using Image-pro plus 6.0 to obtain the dynamic and static globularisation fractions of α phase, and α grain with aspect ratio less than 2 is defined as globularized grain. The globularization fraction of α phase, G_α, can be expressed as

$$G_\alpha = S_g / S_\alpha \tag{1}$$

where S_g denotes the area of globularized α grains (μm^2), and S_α denotes the area of α grains (μm^2). In order to ensure the statistic relevance of quantitative results, three micrographs were selected for quantitative analysis under each process parameter and their average value was finally taken as the quantitative result.

The EBSD data were analyzed by HKL-Channel 5 software. In the present work, grain boundaries with misorientation angles between 2° and 15° are identified as low angle grain boundaries (LABs), which were outlined using white lines in the inverse pole figure (IPF) map of α phase and in the band contrast (BC) map of β phase. And those with misorientation angles over 15° are identified as high angle grain boundaries (HABs), which were outlined using black lines.

In addition, the correlation coefficient (R) and mean absolute relative error (MARE) were used to describe the prediction performance of the kinetics models, and the expressions are as follows:

$$R = \frac{\sum_{i=1}^{N}(E_i - \overline{E})(C_i - \overline{C})}{\sqrt{\sum_{i=1}^{N}\left(E_i - \overline{E}\right)^2}\sqrt{\sum_{i=1}^{N}\left(C_i - \overline{C}\right)^2}} \tag{2}$$

$$\mathrm{MARE} = \frac{1}{N}\sum_{i=1}^{N}\left|\frac{E_i - C_i}{E_i}\right| \times 100\% \tag{3}$$

where N is the total number of data, E_i and $\overline{E}$ are the experimental data and the average value of E, respectively, C_i and $\overline{C}$ are the predicted value of the model and the average value of C, respectively.

3 Results and discussion

3.1 Effect of deformation parameters on microstructure

Figure 2 shows the effect of deformation temperature on the microstructure of TC17 alloy deformed at the true strain of 0.22 and strain rate of 1 s^{-1}. From Figs. 2(a−c), it can be observed that the volume fraction of α phase decreases gradually as the deformation temperature approaches the β transition temperature. In addition, the globularization of α lamellae also depends on the deformation temperature. Globularization fractions corresponding

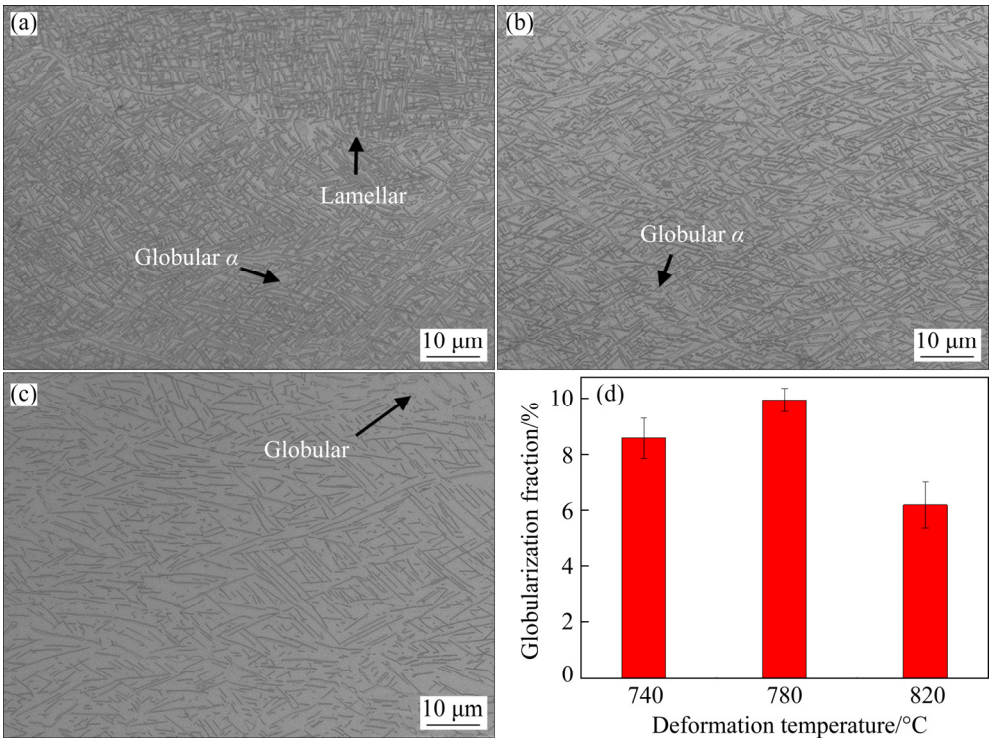

Fig. 2 Optical microstructures of TC17 alloy deformed at strain rate of 1 s^{-1} and strain of 0.22 with different deformation temperatures ((a) 740 °C; (b) 780 °C; (c) 820 °C) and globularization fraction of α phase (d)

to the deformation temperatures of 740, 780 and 820 °C are 8.59%, 9.95% and 6.20%, respectively, as shown in Fig. 2(d). As the deformation temperature rises from 740 to 780 °C, the diffusion is accelerated and lamellar globularization is further activated with increasing deformation temperature [26]. While deformation temperature increases further to 820 °C, which is more close to the β transition temperature, the volume fraction of α phase decreases and β phase dominates the deformation process. Therefore, α lamellae cannot obtain sufficient energy to fragment and the globularization fraction of α phase decreases.

Figure 3 shows the effect of strain on the microstructure of TC17 alloy deformed at the deformation temperature of 740 °C and strain rate of 1 s^{-1}. From Fig. 3(a), it can be observed that α lamellae are still interweaved, only a small amount of globular α phases appear at strain of 0.36, and the globularization fraction of α phase is only 10.34% according to the quantitative result in Fig. 3(d). In addition, the α lamellae rotate towards direction vertical to compression axis (CA) and a few α lamellae are bended after deformation. When the strain increases to 0.69, the α lamellae rotate further and many lamellae are finally parallel to the direction vertical to CA, as shown in Fig. 3(b); more α lamellae break into rods and the globularization fraction of α phase increases to 15.43%. JIA et al [27] studied the dynamic globularization kinetics of Ti−22Al−25Nb with lamellar microstructure during hot deformation and pointed out that large strain would lead to high dynamic globularization fraction. In conclusion, larger deformation degree can provide more stored energy and substructures, which is beneficial to the fragmentation of α lamellae. However, as the strain increases to 1.20, the globularization fraction of α phase decreases to 14.28%, as shown in Fig. 3(d). The reason is that α lamellae and the formed globularized particles are further stretched in the direction perpendicular to CA as the deformation continues, and the α phase are almost parallel to the direction vertical to CA, as shown in Fig. 3(c). Therefore, the globularization of α phase decreases.

Figure 4 shows the effect of strain rate on the microstructure of TC17 alloy deformed at the deformation temperature of 740 °C and strain of 0.22. With increasing strain rates from 0.01 to 1 s^{-1}, it can be observed that the spacing distance between α lamellae decreases. However, the average length

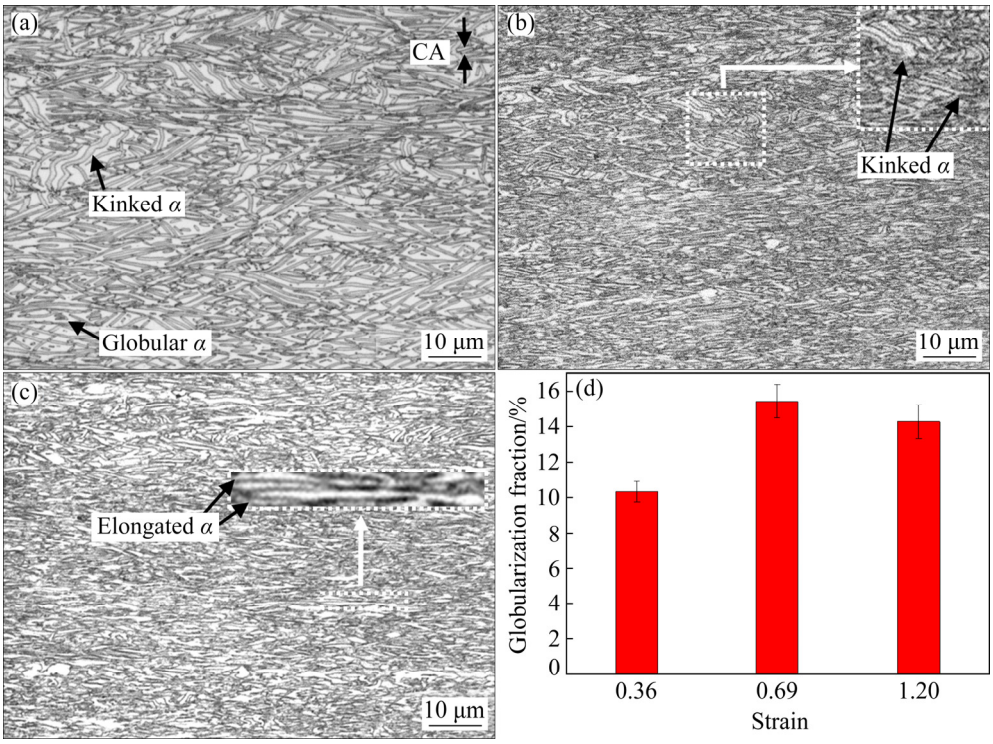

Fig. 3 Optical microstructures of TC17 alloy deformed at temperature of 740 °C and strain rate of 1 s^{-1} with different strains ((a) 0.36; (b) 0.69; (c) 1.20) and globularization fraction of α phase (d)

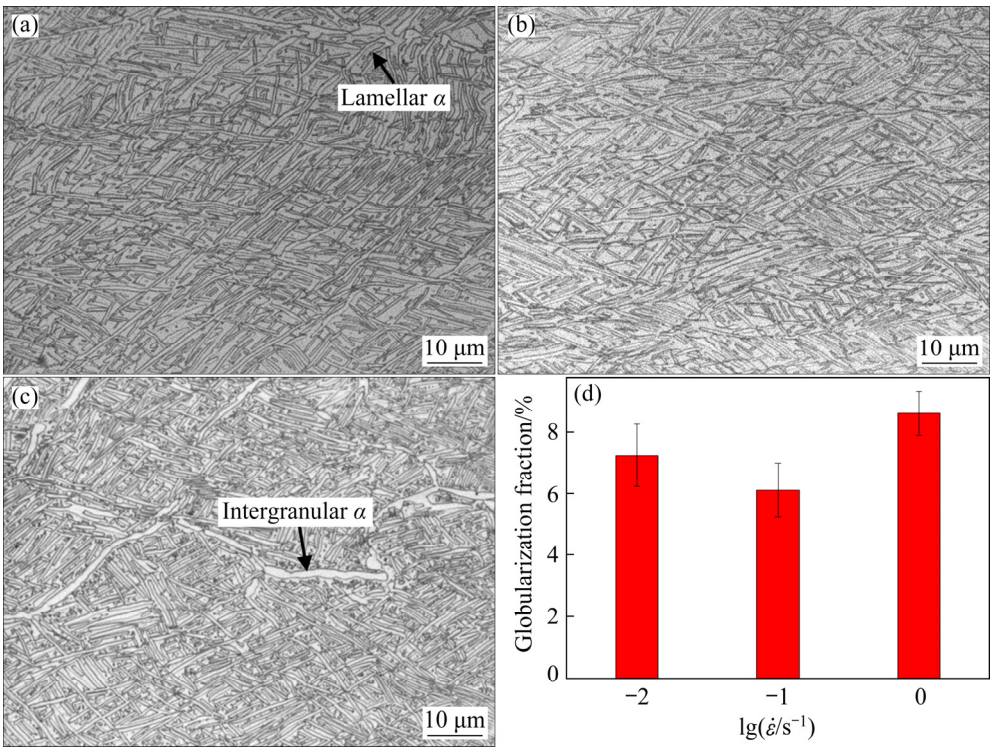

Fig. 4 Optical microstructures of TC17 alloy deformed at temperature of 740 °C and strain of 0.22 with different strain rates ((a) 0.01 s^{-1}; (b) 0.1 s^{-1}; (c) 1 s^{-1}) and globularization fraction of α phase (d)

of the α lamellae increases from 3.7 to 5.0 μm as the strain rate increases. The reason is that most of α lamellae rotate and fragment insufficiently due to the shorter deformation time at higher strain rate, and finally α lamellae with large length exist. The microstructure at different strain rates in the present

work shows the similar dynamic globularization behaviors, as observed in Fig. 4. From the quantitative result in Fig. 4(d), the globularization fractions are 7.25%, 6.12% and 8.59% at strain rates of 0.01, 0.1 and 1 s^{-1}, respectively. The reason why the effect of strain rate on dynamic globularization is not obvious is that there is little difference in deformation time due to the small true strain (0.22). In addition, the deformation temperature is low (740 °C), and the globularization of α phase is limited and more related to local rotation of the substructures in the lamella, leading to the fragmentation of α lamellae. Thus, the fragmentation seems to be more dependent on the strain rather on the time. Therefore, the strain rates have little effect on the dynamic globularization of α phase in the present work.

3.2 Effect of heat treatment and pre-deformation parameters on microstructure

After deformation, substructures formed in titanium alloys during deformation are beneficial to globularization of lamellar α during heat treatment due to the increasing stored energy. Figure 5 shows the effect of heat treatment temperature on the microstructure of deformed TC17 alloy heat treated for 1 h with the pre-deformation parameters of 740 °C, strain rate of 1 s^{-1} and strain of 0.22. From Fig. 5, it can be observed that heat treatment temperature has great influence on the evolution of the globularization of α phase. With the increase of heat treatment temperature, the $\alpha \rightarrow \beta$ phase transformation is promoted and thus the volume fraction of α phase decreases. Meanwhile, the static globularization is a typical elemental diffusion process, which is accelerated with increasing heat treatment temperature [13,28]. Therefore, with increasing heat treatment temperature, the migration of β stabilized elements into α phase is accelerated, which is beneficial to the boundary splitting, termination migration and Ostwald ripening of α phase due to the fast element diffusion [16,29]. According to the quantitative results in Fig. 5(d), the globularization fractions are 12.37%, 13.80% and 23.99% at heat treatment temperatures of 720, 760 and 800 °C, respectively. Therefore, the higher the heat treatment temperature is, the faster the globularization of the α phase is.

Figure 6 shows the effect of heat treatment time on the microstructure of deformed TC17 alloy heat-treated at 800 °C with the pre-deformation parameters of 740 °C, strain rate of 1.0 s^{-1} and strain of 1.20. It can be observed that the number, size and globularization fraction of α phase vary

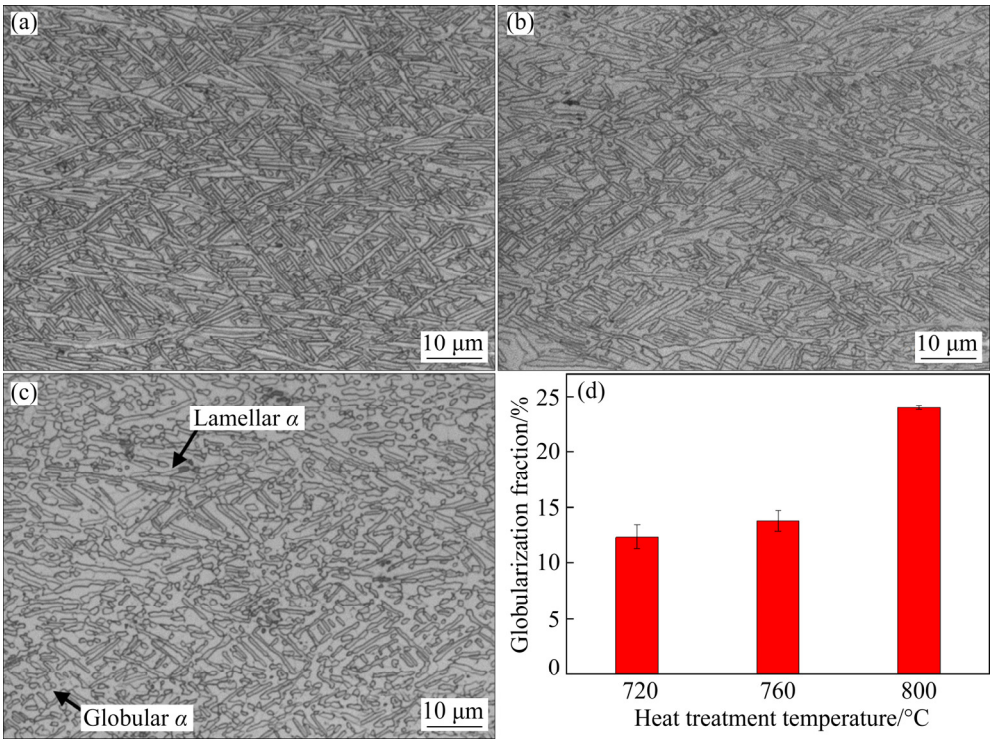

Fig. 5 Optical microstructures of TC17 alloy heat-treated for 1 h at different heat treatment temperatures ((a) 720 °C; (b) 760 °C; (c) 800 °C) and globularization fraction of α phase (d)

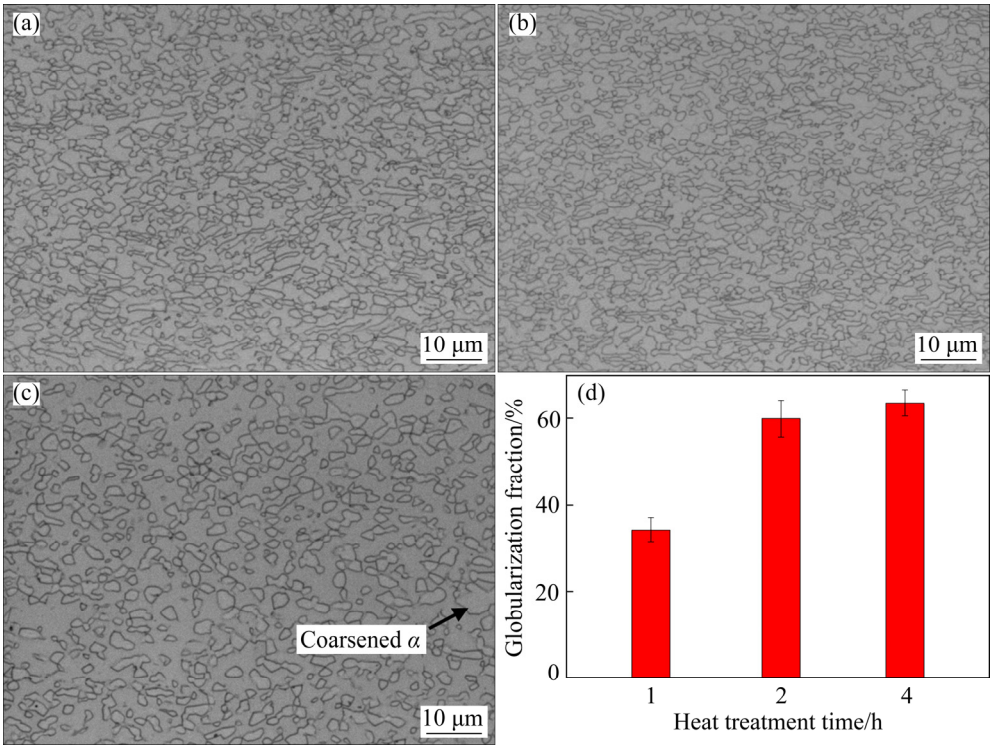

Fig. 6 Optical microstructures of TC17 alloy heat-treated at 800 °C for different time ((a) 1 h; (b) 2 h; (c) 4 h) and globularization fraction of α phase (d)

significantly for tested heat treatment time. With increasing heat treatment time, the α lamellae are fragmented driven by diffusion due to dissolution and coarsening of the formed particles, and finally the globularization of α phase is further completed. From the quantitative result in Fig. 6(d), the globularization fractions of α phase are 34.29%, 59.95% and 63.63% at heat treatment time of 1, 2 and 4 h, respectively, which indicates that globularization is promoted as the heat treatment time increases.

Figure 7 shows the effect of pre-deformation temperature on the microstructure of deformed TC17 alloy heat-treated at 800 °C for 1 h with the pre-deformation strain of 0.22 and strain rate of 1 s^{-1}. By comparing the deformed microstructure in Fig. 2 with the heat-treated microstructure in Fig. 7, the globularization of α phase is further promoted after heat treatment. The globularization fractions are 23.41%, 17.99% and 16.88% at the pre-deformation temperatures of 740, 780 and 820 °C, as shown in Fig. 7(d), which indicates that the static globularization fraction decreases with increasing pre-deformation temperature. It can be observed that higher deformation temperature leads to lower fraction of α phase from Fig. 2. The microstructure can obtain more stored energy at lower deformation temperature due to more α phase and weaker dynamic recovery [30], which is beneficial to static globularization during heat treatment, so there are more globular α phases at the lower pre-deformation temperature of 740 °C, as shown in Fig. 7(a). Therefore, decreasing pre-deformation temperature promotes the static globularization in the present work.

Figure 8 shows the effect of pre-deformation strain on the microstructure of TC17 alloy heat-treated at 760 °C for 1 h with the pre-deformation temperature of 740 °C and strain rate of 1 s^{-1}. Compared with the deformed microstructure in Fig. 3, the globularization of α phase is promoted after heat treatment. When the pre-deformation strain is 0.36, many grooves occur on the surface of lamellar α after heat treatment, as shown by the arrow in Fig. 8(a). More kinked α phases are formed after deformation with increasing strain and the kinked α phases reduce the elemental diffusion distance so that the termination migration is easy to occur during heat treatment [31], and thus the static globularization of α phase is further promoted with increasing pre-deformation strain. Meanwhile, the kinked α can provide driving force for Ostwald

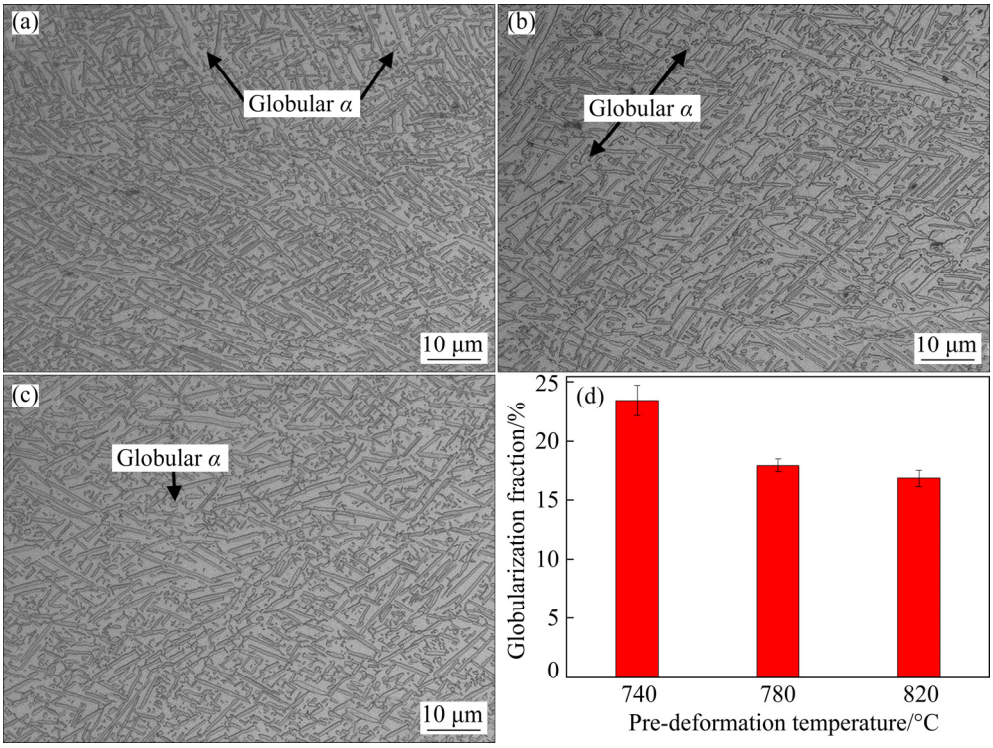

Fig. 7 Optical microstructures of TC17 alloy heat-treated at 800 °C for 1 h with different pre-deformation temperatures ((a) 740 °C; (b) 780 °C; (c) 820 °C) and globularization fraction of α phase (d)

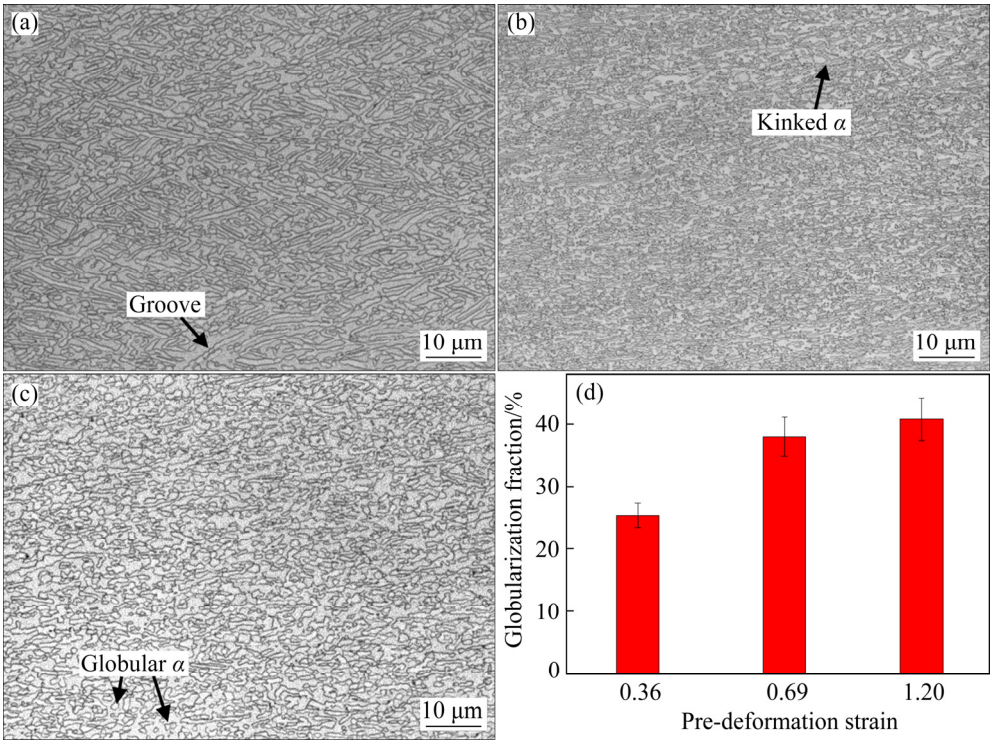

Fig. 8 Optical microstructures of TC17 alloy heat-treated at 760 °C for 1 h with different pre-deformation strains ((a) 0.36; (b) 0.69; (c) 1.20) and globularization fraction of α phase (d)

ripening due to the large curvature at the bend [32], which is beneficial to the growth and coarsening of α phase. The kinked α can store more substructures and energy at larger strain, which can further promote the termination migration and Ostwald ripening of α phase. According to the quantitative

result in Fig. 8(d), static globularization fractions of α phase are 25.42%, 38.05 and 40.85% at the pre-deformation strains of 0.36, 0.69 and 1.20, respectively. Therefore, the increase of pre-deformation strain is beneficial to the static globularization of α phase.

Figure 9 shows the effect of pre-deformation strain rate on the microstructure of TC17 alloy heat-treated at 800 °C for 1 h with the pre-deformation temperature of 740 °C and strain of 0.22. It can be concluded that strain rate has little effect on dynamic globularization in the present work, as shown in Fig. 4. However, the strain rate has considerable effect on the static globularization of α phase during heat treatment, as shown in Fig. 9. After heat treatment, the globularization is promoted compared to the deformed microstructure in Fig. 4. The promotion of heat treatment on globularization is not obvious when the pre-deformation strain rate is 0.01 s^{-1}, and the globularization fraction of α phase increase from 7.25% to 10.22% after heat treatment. When the pre-deformation strain rate is high, the fragmentation of α phase is promoted greatly after heat treatment, and more globular α phases are observed in Figs. 9(b, c). The globularization fractions of α phase increase from 6.12% to 21.49% and from 8.59% to 23.41% at the pre-deformation strain rates of 0.1 and 1 s^{-1}, respectively. The reason is that dynamic recovery is sufficient at lower strain rate during deformation, which causes less stored energy and substructures. Therefore, higher pre-deformation strain rate is beneficial to the static globularization during heat treatment due to more stored energy and substructures.

3.3 Evolution mechanism of intra-α boundary

Boundary splitting is a crucial mechanism of lamellar globularization, which consists of the formation of intra-α boundary, and the separation along the boundary started at the triple point due to the chemical potential gradient caused by interface curvature [16,33]. Among the mechanisms to form intra-α boundaries, shear band [34] and continuous dynamic recrystallization [18,19] have been observed. Therefore, EBSD measurement was carried out to further clarify the evolution mechanism of intra-α boundary during deformation and heat treatment of TC17 alloy in the present work.

Figure 10(a) shows the microstructure of TC17 alloy deformed at 740 °C and strain rate of 1 s^{-1} and strain of 0.22. After deformation, a few of α lamellae are fragmented and globularized, and some

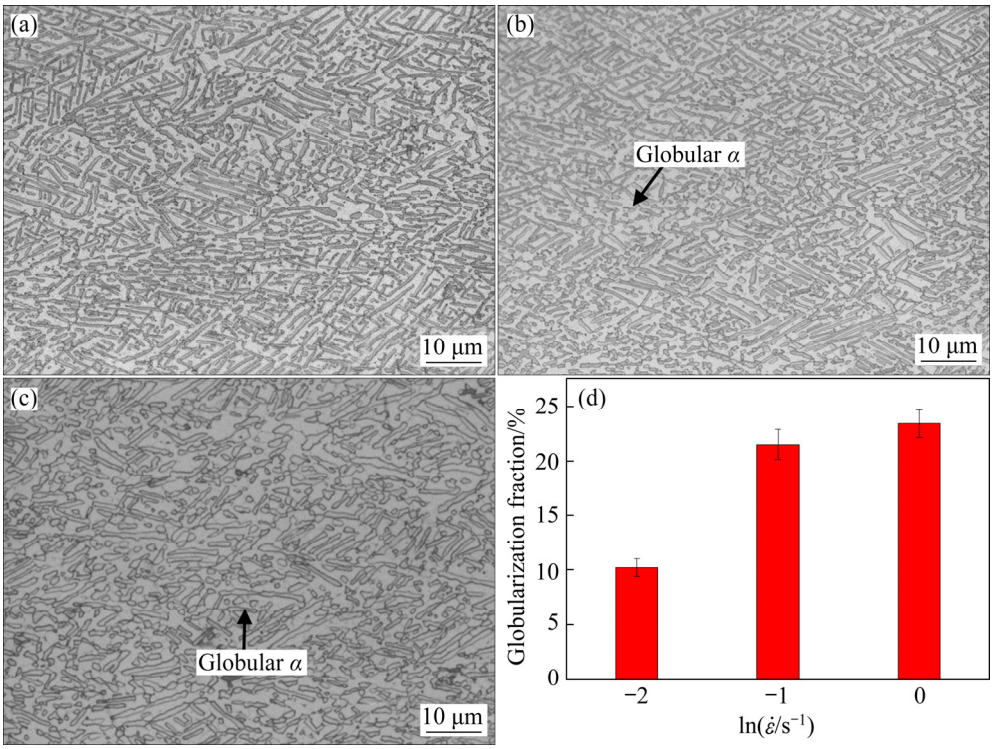

Fig. 9 Optical microstructures of TC17 alloy heat-treated at 800 °C for 1 h with different pre-deformation strain rates ((a) 0.01 s^{-1}; (b) 0.1 s^{-1}; (c) 1 s^{-1}) and globularization fraction of α phase (d)

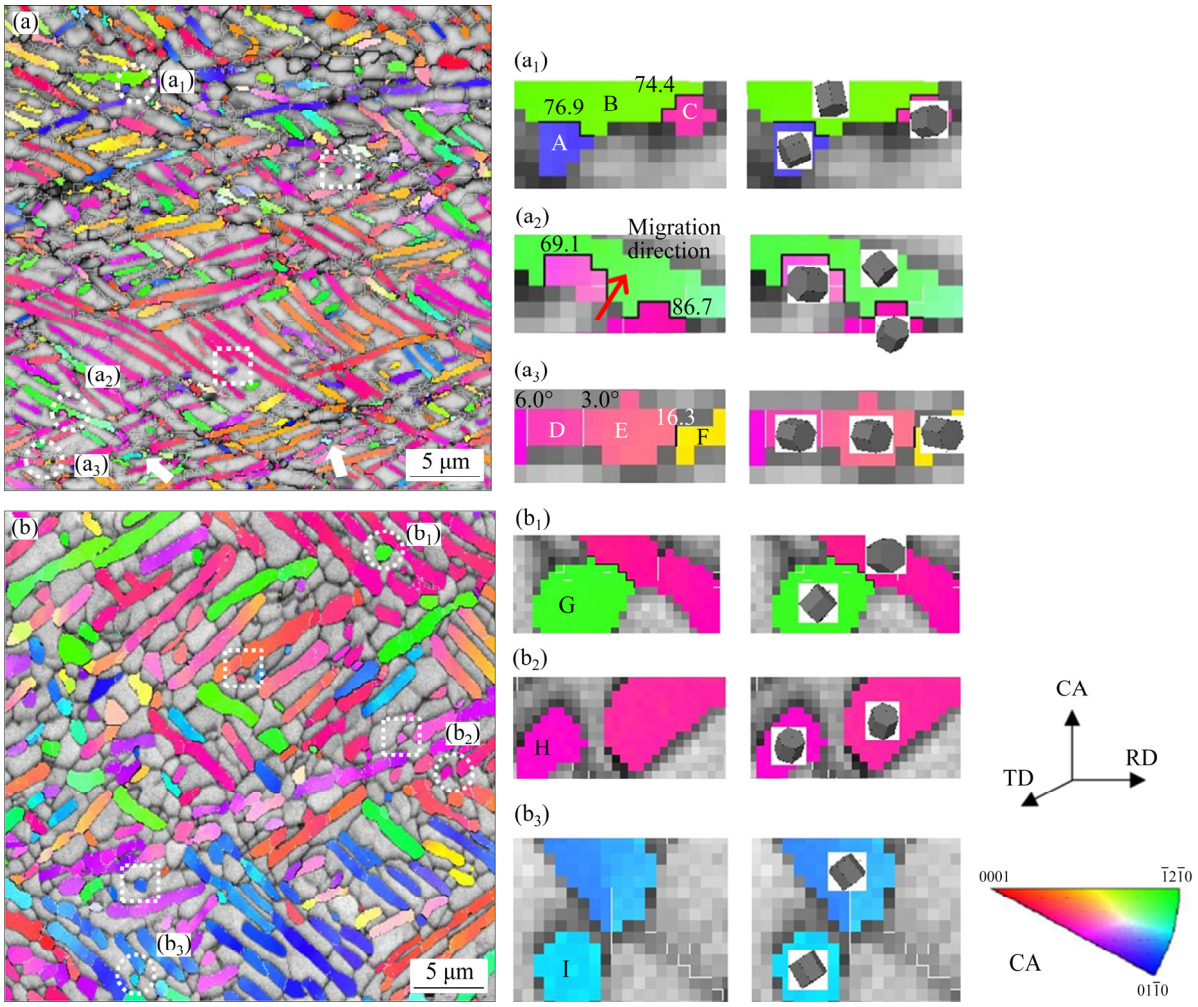

Fig. 10 Overlap maps of IPF for α phase and BC for β phase of TC17 alloy deformed at deformation temperature of 740 °C, strain rate of 1 s^{-1} and strain of 0.22 (a) and subsequently heat-treated at 800 °C for 1 h (b): (a_1−a_3, b_1−b_3) Local α phase

globular α grains are formed, as shown by the white squares in Fig. 10(a). Meanwhile, a large number of low angle grain boundaries (LABs) and high angle grain boundaries (HABs) are generated in α lamellae. The α lamellae are divided into several grains or subgrains by these intra-α boundaries, as shown by the white arrows in Fig. 10(a). These HABs are beneficial to the separation of α lamellae due to high interfacial energy, which can promote the diffusion of the β stabilized elements such as Mo and Cr to the α lamellae [35]. However, the element diffusion process is incomplete due to the short deformation time, the HABs cannot migrate sufficiently and thus the globularization of α lamellae is limited.

The deformed TC17 alloy is heat-treated at 800 °C for 1 h and the microstructure is shown in Fig. 10(b). The lamellae are coarsened after heat treatment and more globular α phases are formed, as shown by the white square in Fig. 10(b). In addition, it can be observed that amount of the HABs in α lamellae decreases obviously. Figure 11 shows the grain boundary misorientation for α phase of the deformed and heat-treated TC17 alloy. As shown in Fig. 11, the fraction of HABs in the α lamellae of deformed TC17 alloy is 50.2%. However, HABs are hardly formed in the α lamellae and the fraction of HABs decreases to 24.4% after heat treatment. This is because the migration of α/β phase boundaries consumes the HABs formed by deformation, which causes the penetration of β phase into α lamellae. Finally, the α lamellae are separated and the intra-α boundaries are transformed into the α/β phase boundaries. Thus, the amount of HABs in α lamellae decreases after heat treatment.

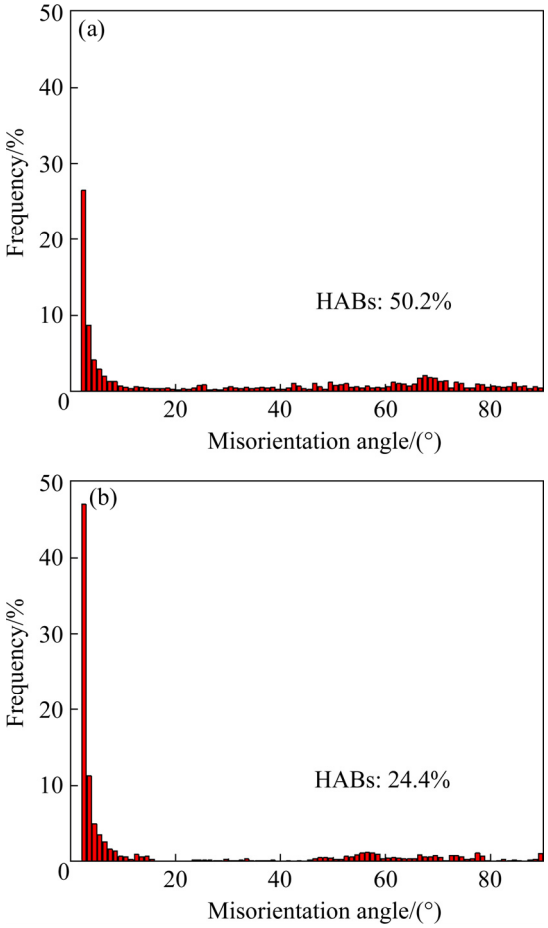

Fig. 11 Distribution of grain boundary misorientation for α phase of TC17 alloy deformed at 740 °C, strain rate of 1 s^{-1} and strain of 0.22 (a) and subsequently heat-treated at 800 °C for 1 h (b)

Figures 10(a, b) show a further investigation of the mechanism for evolution of the intra-α boundaries. Deformation produces many defects such as dislocations in α lamellae, which provides energy for nucleation. As shown in Fig. 10(a_1), the misorientation angles between Grain A and Grain B, and between Grain C and Grain B are 76.9° and 74.4°, respectively. The crystal orientation of each grain is shown in the right side of Fig. 10(a_1). It can be found that the crystal orientation of Grain A and Grain C is greatly different from those of original Grain B, which means that the nucleation of Grain A and Grain C is random, and the size of Grain A and Grain C is small. This is the typical nucleation way of discontinuous dynamic recrystallization (DDRX) [36]. Then, the recrystallized grains grow and the intra-α boundary migrates inward into the α lamella, as shown in Fig. 10(a_2). Eventually, this type of intra-α boundary is separated into two independent grain boundaries in α lamella and divide the original α lamella into several grains. However, the boundary migration and globularization process are insufficient due to the short deformation time, and this process is further promoted during heat treatment. Figure 10(b_1) shows that the globularized-α Grain G has very different orientation with nearby grains after heat treatment, which may be related to further evolution of the nucleation formed by DDRX or static recrystallization during heat treatment.

The recrystallization image is provided by EBSD and HKL channel 5 software, as shown in Fig. 12. The grain is classified as recrystallized grain when the misorientation in a grain is <2°, which is represented in blue in Fig. 12. The yellow grains are the substructured grains with the misorientation between 2° and 15°. Otherwise, the grains with misorientation exceeding 15° are classified as deformed grains which are represented in red. It can be seen that the fine grains in Figs. 10(a_1, a_2) are recrystallized grains. The fine grains have low misorientation and do not belong to another lamella. Therefore, the fine grains formed at the interface of lamella are nucleated via DDRX.

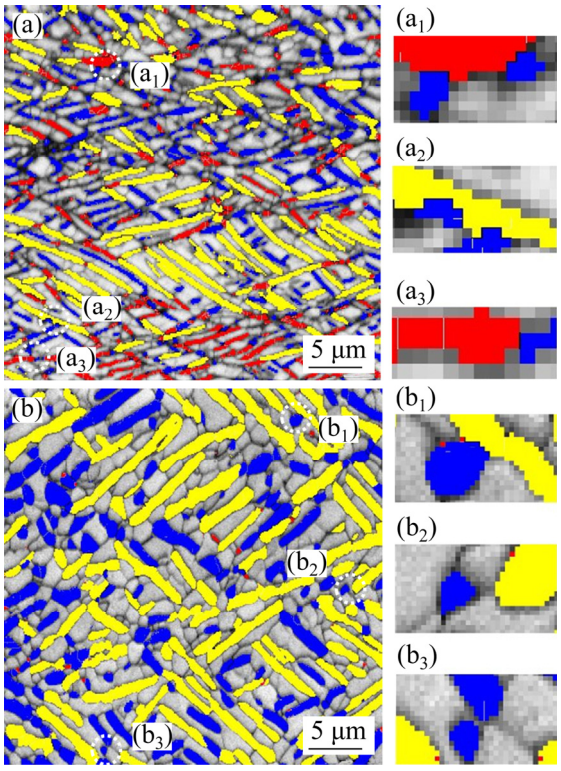

Fig. 12 Overlap maps of recrystallization image for α phase and BC for β phase of TC17 alloy deformed at 740 °C, strain rate of 1 s^{-1} and strain of 0.22 (a) and subsequently heat-treated at 800 °C for 1 h (b)

Continuous dynamic recrystallization (CDRX) is also an important globularization mechanism of TC17 alloy during deformation, and its typical process is crystal rotation [20]. A typical α lamella is chosen to study. From Fig. 10(a_3), the change of crystal orientation of the α lamella is observed. The Euler angles of Substructures D, E and F are calculated as [φ=79.6°, θ=43.4°, ψ=22.5°], [φ=80.5°, θ=44.4°, ψ=16.9°] and [φ=80.5°, θ=43.0°, ψ=0.0°], respectively, which indicates a continuous crystal rotation process around Z axis of the hexagonal closepacked structure (hcp). Then, LABs and HABs are formed in this α lamella, and the misorientation angles among substructures are 6.0°, 3.0° and 16.3°. Finally, the CDRX grain is formed when the misorientation angle exceeds 15°, as shown in Fig. 12(a_3). Moreover, the basal slip or pyramidal slip is easy to activate so that the crystal rotation process can be further promoted, then the LABs are transformed to HABs gradually during heat treatment, and finally, the α lamella is separated [37]. As shown in Figs. 10(b_2, b_3) and Figs. 12(b_2, b_3), the globularized-α Grains H and I have similar misorientation with the original lamella, which may be related to the further separation of the nucleation formed by CDRX during heat treatment.

EBSD measurement was carried out to further investigate the effect of pre-deformation strain rate on static globularization, as shown in Fig. 13. As seen from Figs. 10(b) and 13, the α phases mainly consist of globular α grains and short α rods at the pre-deformation strain rates of 1 and 0.1 s^{-1}. However, for the specimen deformed at the strain rate of 0.01 s^{-1}, most of α phases still retain lamellar structure, which is consistent with the quantitative results in Fig. 9(d).

The grain boundary misorientation distribution of α phase is shown in Fig. 14. The fraction of HABs for α phase at pre-deformation strain rate of 1 s^{-1} is 24.4%, which is much smaller than 32.8% at strain rate of 0.1 s^{-1} and 32.3% at strain rate of 0.01 s^{-1}. The reason is that faster boundary splitting process leads to the transformation from intra-α boundary to α/β phase boundary at the pre-deformation strain rate of 1 s^{-1}. Otherwise, the microstructure at the pre-deformation strain rate of 0.1 s^{-1} has similar HABs fraction but higher globularization fraction compared with the microstructure at strain rate of 0.01 s^{-1}. In the present work, the deformation time is short due to the small strain (0.22), and the recrystallized grains generated by DDRX during deformation have high misorientation and grain boundary energy, which is beneficial to the growth of recrystallized grains and boundary migration during heat treatment [38]. But the recrystallized grains associated with CDRX are generated by continuous crystal rotation, which leads to lower misorientation compared with DDRX at the small strain of 0.22, and thus the boundary splitting process during heat treatment is relatively slow, and HABs are preserved and globularization fraction slowly increases. Therefore, the dominant recrystallization mechanism during deformation is gradually changed from CDRX to DDRX as the strain rate increases from 0.01 to 1 s^{-1} in the present work.

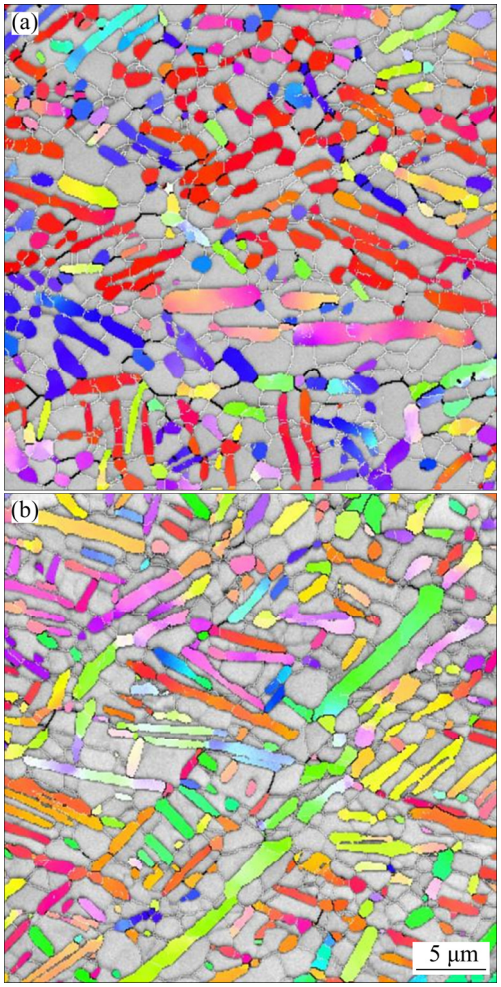

Fig. 13 Overlap maps of IPF for α phase and BC for β phase of TC17 alloy deformed at 740 °C and strain of 0.22 and subsequently heat-treated at 800 °C for 1 h with different pre-deformation strain rates: (a) 0.1 s^{-1}; (b) 0.01 s^{-1}

The formation of globularized α grains that have large misorientation with nearby lamella is associated with DDRX during deformation at high strain rate, and the fine particles formed by DDRX grow and are eventually separated from the original lamella during heat treatment. In addition, the formation of globularized α grains that have small misorientation with nearby lamella is associated with CDRX during deformation at low strain rate. The subgrains generated by CDRX during deformation further rotate after heat treatment, and are eventually separated. The schematic diagram of the whole globularization process is shown in Fig. 15.

3.4 Model of dynamic globularization kinetics

The globularization of α phase can be interpreted as a type of recrystallization, and a critical strain is assumed for the initiation of dynamic globularization. Dynamic globularization fraction approximately increases with strain in a sigmoid and can be fitted with JMAK model [8−10]. In the present work, a modified JMAK model is developed to describe the dynamic globularization kinetics. The model is expressed as

$$f_{\mathrm{Dg}} = 1 - \exp[-k(\varepsilon - \varepsilon_{\mathrm{c}})^{n}] \tag{4}$$

where f_{Dg} denotes the dynamic globularization fraction, ε_{c} is the critical strain for initiation of dynamic globularization, n is the Avrami exponent, and k is the kinetic constant and temperature-dependent factor.

However, the critical strain (ε_{c}) in Eq. (4) is generally obtained by fitting, which has no clear physical meaning and limits the prediction performance of the model. Dynamic globularization is closely related to recrystallization and it is an important factor of flow softening [39,40]. Therefore, in the present work, ε_{c} is obtained from the flow curve by the P−J methods [41], and the critical stress corresponds to the point where the second derivative of θ−σ curve is zero:

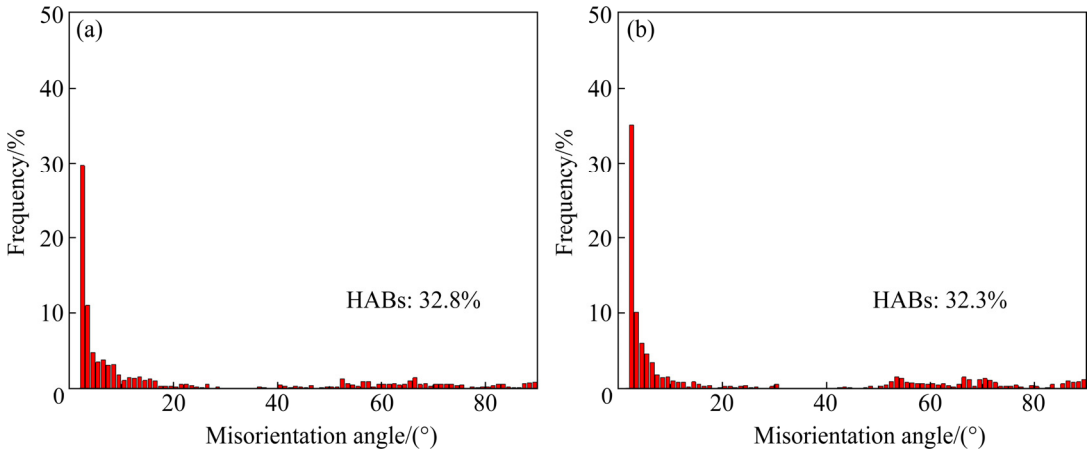

Fig. 14 Distribution of grain boundary misorientation for α phase of TC17 alloy deformed at 740 °C and strain of 0.22 and subsequently heat-treated at 800 °C for 1 h with different pre-deformation strain rates: (a) 0.1 s^{-1}; (b) 0.01 s^{-1}

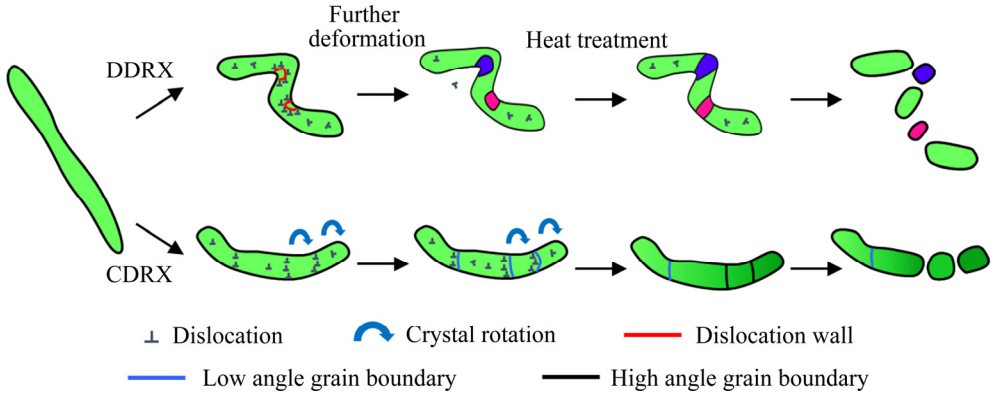

Fig. 15 Schematic diagram of globularization mechanism of TC17 alloy

$$\frac{\partial}{\partial\sigma}\left(\frac{\partial\theta}{\partial\sigma}\right)=0 \tag{5}$$

where θ denotes work hardening rate ($\theta=\mathrm{d}\sigma/\mathrm{d}\varepsilon$), and σ is the flow stress (MPa).

The critical strain can be correlated to the Zener−Hollomon parameter (Z) which incorporates both deformation temperature and strain rate. And the critical strain can be generally expressed as a power-law function of Z [42]:

$$\varepsilon_c=AZ^b \tag{6}$$

$$Z=\dot{\varepsilon}\exp[Q/(RT)] \tag{7}$$

where A and b are constants, $\dot{\varepsilon}$ is the strain rate (s^{-1}), Q is the deformation activation energy (567.7 kJ/mol [43]), R is the molar gas constant (8.314 J/(mol·K)), and T is the thermodynamic temperature (K).

The critical strains obtained from Eq. (5) are plotted on a double-logarithmic scale as a function of Z, as shown in Fig. 16. Then, linear regression method is used to estimate the constants in Eq. (6). Hence, the equation of critical strain and Z parameter for the present alloy can be obtained:

$$\varepsilon_c=7.431\times10^{-4}Z^{0.05944} \tag{8}$$

The following equation can be obtained by taking the logarithm of both sides of Eq. (4):

$$\ln\left[\ln\left(\frac{1}{1-f_{\mathrm{Dg}}}\right)\right]=\ln k+n\ln(\varepsilon-\varepsilon_c) \tag{9}$$

It can be found that $\ln\{\ln[1/(1-f_{\mathrm{Dg}})]\}$ and $\ln(\varepsilon-\varepsilon_c)$ have a good linear relationship using the quantitative results at the deformation temperature of 740 °C, as shown in Fig. 17.

The slope and intercept of Eq. (9) are calculated to be 0.5026 and −1.56514. Thus, the dynamic globularization kinetics of TC17 alloy at a deformation temperature of 740 °C can be described as follows:

$$f_{\mathrm{Dg}}=1-\exp[-0.2091(\varepsilon-\varepsilon_c)^{0.5026}] \tag{10}$$

$$Z=\dot{\varepsilon}\exp[567700/(RT)] \tag{11}$$

The comparison between the predicted values calculated by Eq. (10) and experimental values is shown in Fig. 18. The correlation coefficient reaches more than 95% through calculation and the mean absolute relative error (MARE) between the experimental and predicted values is 10.67%, which indicates that the model has good predictability.

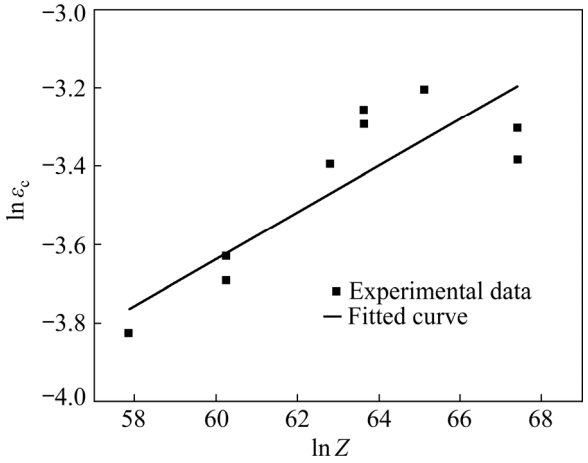

Fig. 16 Relationship between $\ln\varepsilon_c$ and $\ln Z$ of TC17 alloy

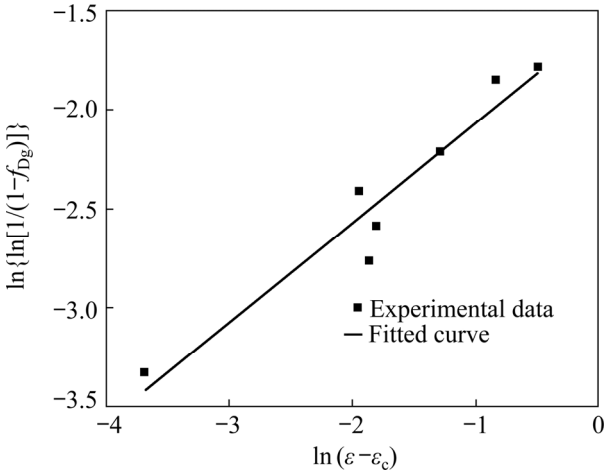

Fig. 17 Relationship between $\ln\{\ln[1/(1-f_{\mathrm{Dg}})]\}$ and $\ln(\varepsilon-\varepsilon_c)$ of TC17 alloy deformed at 740 °C

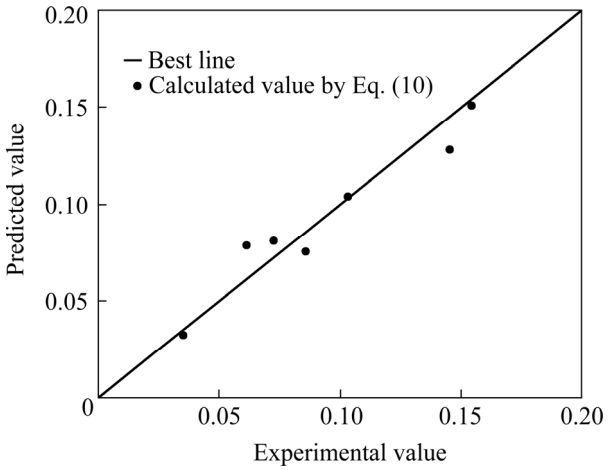

Fig. 18 Comparison between experimental value and predicted value calculated by Eq. (10)

3.5 Model of static globularization kinetics

JMAK model also has good application in predicting static recrystallization [44,45]. And it is also used to predict static globularization kinetics due to the similarity between static globularization and static recrystallization [13,37]. Another modified JMAK model is developed in the present work to describe static globularization kinetics, and the model is expressed as

$$f = 1 - \exp(-k't^n) \tag{12}$$

where f denotes the globularization fraction, k' is globularization rate constant, n is Avrami exponent and t is heat treatment time. However, the static globularization is a complex process which is related to pre-deformation strain, strain rate, heat treatment temperature and time as shown in Section 3.2. Equation (12) only shows the relationship between globularization fraction and heat treatment time, and thus a modified JMAK model is used to describe the process of static globularization [46]:

$$f = 1 - \exp\left[-k'\left(\frac{t}{t_{0.5}}\right)^n\right] \tag{13}$$

The parameter $t_{0.5}$ denotes the time required to reach 50% globularization fraction. It is mainly influenced by strain, strain rate and heat treatment temperature, so it can be expressed as [46]

$$t_{0.5} = A'\varepsilon^{-a}\dot{\varepsilon}^{-p}\exp[Q/(RT)] \tag{14}$$

where A' is material constant, and a and p are constants. The $t_{0.5}$ is substituted in Eq. (13) and then the logarithm of both sides is taken to obtain the following equation:

$$\ln\{\ln[1/(1-f)]\} = na\ln\varepsilon + n\ln t + np\ln\dot{\varepsilon} - n\ln A' + \ln k' - nQ/(RT) \tag{15}$$

In order to simplify the model and couple the influence of pre-deformation strain ε, strain rate $\dot{\varepsilon}$ and heat treatment time t, the constants a and p are assumed to be equal to 1, and the following equation is obtained:

$$\ln[\ln(1/(1-f))] = n\ln(\varepsilon\dot{\varepsilon}t) - n\ln A' + \ln k' - nQ/(RT) \tag{16}$$

The parameter $\ln k' - n\ln A' - nQ/(RT)$ can be simplified to a constant when the heat treatment temperature is determined. Thus, the linear fitting method can be used to obtain the relationship between $\ln[\ln(1/(1-f))]$ and $\ln(\varepsilon\dot{\varepsilon}t)$. Quantitative data at a heat treatment temperature of 800 °C are put into Eq. (16) and the fitting result is shown in Fig. 19. The slope and intercept of Eq. (16) are calculated to be 0.2722 and −0.5225. Therefore, the static globularization kinetics of TC17 alloy heat-treated at 800 °C can be described by

$$f = 1 - \exp\left[-\exp\left(0.2722\ln(\varepsilon\dot{\varepsilon}t) - 0.5225\right)\right] \tag{17}$$

The comparison between the predicted values calculated by Eq. (17) and experimental values is shown in Fig. 20. The correlation coefficient and the MARE between the experimental and predicted values are 95% and 13.80%, respectively. The modified JMAK model is able to predict the influence of the pre-deformation strain, strain rate and heat treatment time on the static globularization of the α phase.

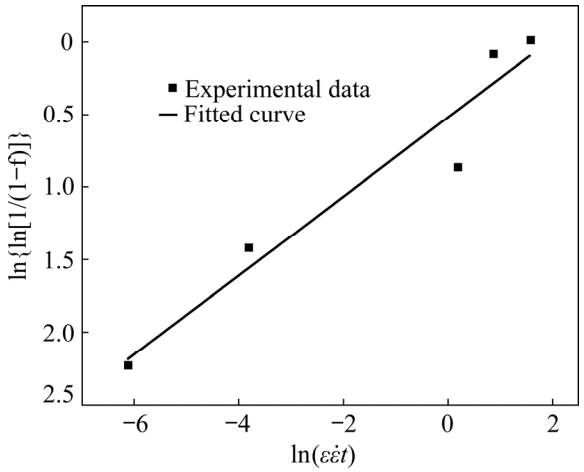

Fig. 19 Relationship between $\ln\{\ln[1/(1-f)]\}$ and $\ln(\varepsilon\dot{\varepsilon}t)$ of TC17 alloy heat-treated at 800 °C

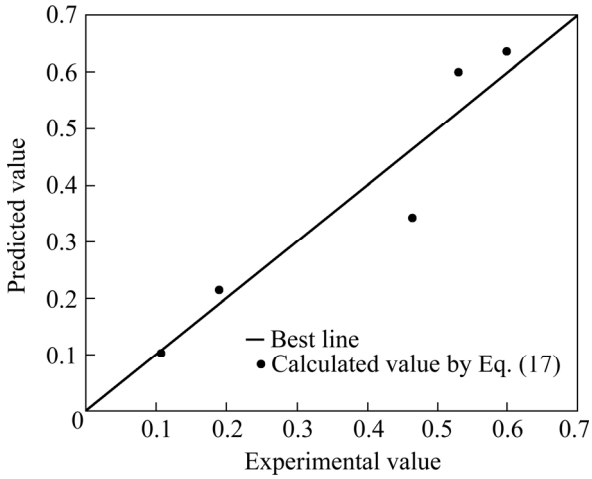

Fig. 20 Comparison between experimental value and predicted value calculated by Eq. (17)

4 Conclusions

(1) The dynamic globularization fraction of TC17 alloy with basketweave microstructure increases first and then decreases with increasing deformation temperature. Increasing true strain can accelerate dynamic globularization but further deformation can elongate α grains and reduce globularization fraction.

(2) The static globularization is promoted with increasing pre-deformation strain and strain rate, heat treatment temperature and time, and decreasing pre-deformation temperature.

(3) The formation and evolution mechanisms of intra-α boundaries are discontinuous dynamic recrystallization (DDRX) and continuous dynamic recrystallization (CDRX). In DDRX, the intra-α boundary is formed by nucleation, which has a high misorientation angle. Then, the boundary migrates inward into the α lamella and finally across the α lamella. In CDRX, the formation of intra-α boundary is caused by crystal rotation, which leads to the transition from low angle boundary to high angle boundary gradually.

(4) The critical strain expressed as a function of Zener−Hollomon parameter is introduced in a modified JAMK model to predict the dynamic globularization kinetics, which makes the model more physical and realistic. The correlation coefficient greater than 95% and the MARE of 10.67% indicate the accuracy of this model.

(5) A modified JMAK model incorporating the influence of pre-deformation strain, strain rate and heat treatment time by introducing the $t_{0.5}$ parameter is developed to predict the static globularization kinetics. The correlation coefficient of 95% and the MARE of 13.80% show good agreement between the model results and experimental measurements.

Acknowledgments

The authors acknowledge the support from the Science Fund for Distinguished Young Scholars from Shaanxi Province, China (No. 2020JC-17), the National Natural Science Foundation of China (No. 51705425), the Research Fund of the State Key Laboratory of Solidification Processing (NWPU), China (No. 2019-QZ-04), and the Fundamental Research Funds for the Central Universities, China (No. 3102019PY007).

References

[1] FRÉOUR S, GLOAGUEN D, FRANÇOIS M, GUILLÉN R. Application of inverse models and XRD analysis to the determination of Ti-17 β-phase coefficients of thermal expansion [J]. Scripta Materialia, 2006, 54(8): 1475−1478.

[2] LUO J, LI L, LI M Q. The flow behavior and processing maps during the isothermal compression of Ti17 alloy [J]. Materials Science and Engineering A, 2014, 606: 165−174.

[3] LI Hui-min, LI Miao-quan, LUO Jiao, WANG Ke. Microstructure and mechanical properties of heat-treated Ti−5Al−2Sn−2Zr−4Mo−4Cr [J]. Transaction of Nonferrous Metals Society of China, 2015, 25(9): 2893−2900.

[4] BANERJEE D, WILLIAMS J C. Perspectives on titanium science and technology [J]. Acta Materialia, 2013, 61(3): 844−879.

[5] ZHU Yan-yan, CHEN Bo, TANG Hai-bo, CHENG Xu, WANG Hua-ming, LI Jia. Influence of heat treatments on microstructure and mechanical properties of laser additive manufacturing Ti−5Al−2Sn−2Zr−4Mo−4Cr titanium alloy [J]. Transactions of Nonferrous Metals Society of China, 2018, 28(1): 36−46.

[6] MA Xiong, ZENG Wei-dong, SUN Yu, WANG Kai-xuan, LAI Yun-jin, ZHOU Yi-gang. Modeling constitutive relationship of Ti17 titanium alloy with lamellar starting microstructure [J]. Materials Science and Engineering A, 2012, 538: 182−189.

[7] WANG Kai-xuan, ZENG Wei-dong, ZHAO Yong-qing, LAI Yun-jin, ZHOU Yi-gang. Dynamic globularization kinetics during hot working of Ti-17 alloy with initial lamellar microstructure [J]. Materials Science and Engineering A, 2010, 527: 2559−2566.

[8] WU Cheng-bao, YANG He, FAN Xiao-guang, SUN Zhi-chao. Dynamic globularization kinetics during hot working of TA15 titanium alloy with colony microstructure [J]. Transactions of Nonferrous Metals Society of China, 2011, 21(9): 1963−1969.

[9] SONG Hong-wu, ZHANG Shi-hong, CHENG Ming. Dynamic globularization kinetics during hot working of a two phase titanium alloy with a colony alpha microstructure [J]. Journal of Alloys and Compounds, 2009, 480: 922−927.

[10] MA Xiong, ZENG Wei-dong, TIAN Fei, ZHOU Yi-gang. The kinetics of dynamic globularization during hot working of a two phase titanium alloy with starting lamellar microstructure [J]. Materials Science and Engineering A, 2012, 548: 6−11.

[11] CHEN Hui-qin, CAO Chun-xiao. Static globularization of TC11 alloy during hot working process [J]. Rare Metal Materials and Engineering, 2011, 40(6): 946−950.

[12] STEFANSSON N, SEMIATIN S L, EYLON D. The kinetics of static globularization of Ti−6Al−4V [J]. Metallurgical and Materials Transactions A, 2002, 33: 3527−3534.

[13] FAN X G, YANG H, YAN S L, GAO P F, ZHOU J H. Mechanism and kinetics of static globularization in TA15 titanium alloy with transformed structure [J]. Journal of Alloys and Compounds, 2012, 533: 1−8.

[14] XU Jian-wei, ZENG Wei-dong, JIA Zhi-qiang, SUN Xin,

ZHOU Jian-hua. Static globularization kinetics for Ti-17 alloy with initial lamellar microstructure [J]. Journal of Alloys and Compounds, 2014, 603: 239−247.

[15] ITO Y, MURAKAMI S, TSUJI N. SEM/EBSD analysis on globularization behavior of lamellar microstructure in Ti−6Al−4V during hot deformation and annealing [J]. Metallurgical and Materials Transactions A, 2017, 48: 4237−4246.

[16] XU Jian-wei, ZENG Wei-dong, MA Hao-yuan, ZHOU Da-di. Static globularization mechanism of Ti-17 alloy during heat treatment [J]. Journal of Alloys and Compounds, 2018, 736: 99−107.

[17] SHARMA G, RAMANUJAN R V, TIWARI G P. Instability mechanisms in lamellar microstructures [J]. Acta Materialia, 2000, 48(4): 875−889.

[18] LI L, LUO J, YAN J J, LI M Q. Dynamic globularization and restoration mechanism of Ti−5Al−2Sn−2Zr−4Mo−4Cr alloy during isothermal compression [J]. Journal of Alloys Compounds, 2015, 622: 174−183.

[19] LI Lian, LI Miao-quan. Evolution characterization of α lamellae during isothermal compression of TC17 alloy with colony-α microstructure [J]. Materials Science and Engineering A, 2018, 712: 637−644.

[20] GAO Yan, MA Guan-qi, ZHANG Xiao-yong, XU Jian-wei. Microstructure evolution and hot deformation behavior of Ti−6.5Al−2Zr−1Mo−1V alloy with starting lamellar structure [J]. Journal of Alloys and Compounds, 2019, 809: 151852.

[21] MATSUMOTO H, NISHIHARA T, IWAGAKI Y, SHIRAISHI T, ONO Y, CHIBA A. Microstructural evolution and deformation mode under high-temperature-tensile-deformation of the Ti−6Al−4V alloy with the metastable α' martensite starting microstructure [J]. Materials Science and Engineering A, 2016, 661: 68−78.

[22] CHONG Y, BHATTACHARJEE T, GHOLIZADEH R, YI J, TSUJI N. Investigation on the hot deformation behaviors and globularization mechanisms of lamellar Ti−6Al−4V alloy within a wide range of deformation temperatures [J]. Materialia, 2019, 8: 100480.

[23] WANG X X, ZHAN M, GAO P F, MA P Y, YANG K, LEI Y D, LI Z X. Deformation mode dependent mechanism and kinetics of dynamic recrystallization in hot working of titanium alloy [J]. Materials Science and Engineering A, 2020, 772: 138804.

[24] LI Xin, DENG Si-ying, WANG Song-wei, SONG Hong-wu, ZHANG Shi-hong, WANG Ke-lu, OUYANG De-lai. Dynamic globularization mechanism during hot working of Ti−6.5Al−3.5Mo−1.5Zr−0.3Si alloy with lamellar microstructure [J]. Materials Characterization, 2021, 171: 110749.

[25] CHEN Ke, LUO Jiao, HAN Wen-chao, LI Miao-quan. Formation and evolution of new α grain boundary and its influence on globularization of α lamellae in TC17 alloy [J]. Journal of Alloys and Compounds, 2020, 848: 156141.

[26] HAO Fang, XIAO Jun-feng, FENG Yong, WANG Yue, JU Jian-tou, DU Yu-xuan, WANG Kai-xuan, XUE Li-nan, NIE Zhi-hua, TAN Cheng-weng. Tensile deformation behavior of a near-α titanium alloy Ti−6Al−2Zr−1Mo−1V under a wide temperature range [J]. Journal of Materials Research and Technology, 2020, 9(3): 2818−2831.

[27] JIA Jian-bo, ZHANG Kai-feng, LU Zhen. Dynamic globularization kinetics of a powder metallurgy Ti−22Al−25Nb alloy with initial lamellar microstructure during hot compression [J]. Journal of Alloys and Compounds, 2014, 617: 429−436.

[28] ZHEREBTSOV S, MURZINOVA M, SALISHCHEV G, SEMIATIN S L. Spheroidization of the lamellar microstructure in Ti−6Al−4V alloy during warm deformation and annealing [J]. Acta Materialia, 2011, 59(10): 4138−4150.

[29] XU Jian-wei, ZENG Wei-dong, SUN Xin, JIA Zhi-qiang, ZHOU Jian-hua. Static coarsening behavior of the lamellar alpha in Ti-17 alloy [J]. Journal of Alloys and Compounds, 2015, 631: 248−254.

[30] MATSUMOTO H, KITAMURA M, LI Yun-ping, KOIZUMI Y, CHIBA A. Hot forging characteristic of Ti−5Al−5V−5Mo−3Cr alloy with single metastable β microstructure [J]. Materials Science and Engineering A, 2016, 611: 337−344.

[31] SEMIATIN S L, CORBETT M W, FAGIN P N, SALISHCHEV G A, LEE C S. Dynamic-coarsening behavior of an α/β titanium alloy [J]. Metallurgical and Materials Transactions A, 2006, 37: 1125−1136.

[32] SHAHANI A J, XIAO X, SKINNER K, PETERS M, VOORHEES P W. Ostwald ripening of faceted Si particles in an Al−Si−Cu melt [J]. Materials Science and Engineering A, 2016, 673: 307−320.

[33] WEISS I, FROES F H, EYLON D, WELSCH G E. Modification of alpha morphology in Ti−6Al−4V by thermomechanical processing [J]. Metallurgical and Materials Transactions A, 1986, 17: 1935−1947.

[34] SESHACHARYULU T, MEDEIROS S C, MORGAN J T, MALAS J C, FRAZIER W G, PRASAD Y V R K. Hot deformation and microstructural damage mechanisms in extra-low interstitial (ELI) grade Ti−6Al−4V [J]. Materials Science and Engineering A, 2000, 279: 289−299.

[35] CABIBBO M, ZHEREBTSOV S, MIRONOV S, SALISHCHEV G. Loss of coherency and interphase α/β angular deviation from the Burgers orientation relationship in a Ti−6Al−4V alloy compressed at 800 °C [J]. Journal of Materials Science, 2013, 48: 1100−1110.

[36] KAPOOR R, BHARAT REDDY G, SARKAR A. Discontinuous dynamic recrystallization in α-Zr [J]. Materials Science and Engineering A, 2018, 718: 104−110.

[37] XU Jian-wei, ZENG Wei-dong, ZHANG Xiao-yong, ZHOU Da-di. Analysis of globularization modeling and mechanisms of alpha/beta titanium alloy [J]. Journal of Alloys and Compounds, 2019, 788: 110−117.

[38] DING R, GUO Z X. Coupled quantitative simulation of microstructural evolution and plastic flow during dynamic recrystallization [J]. Acta Materialia, 2001, 49(16): 3163−3175.

[39] LUO Jiao, YE Peng, HAN Wen-chao, LI Miao-quan. Microstructure evolution and its effect on flow stress of TC17 alloy during deformation in $\alpha+\beta$ two-phase region [J]. Transactions of Nonferrous Metals Society of China, 2019, 29(7): 1430−1438.

[40] LI Jun-ling, WANG Bao-yu, HUANG He, FANG Shuang, CHEN Ping, SHEN Jin-xia. Unified modelling of the flow

behaviour and softening mechanism of a TC6 titanium alloy during hot deformation [J]. Journal of Alloys and Compounds, 2018, 748: 1031−1043.

[41] POLIAK E I, JONAS J J. A one-parameter approach to determining the critical conditions for the initiation of dynamic recrystallization [J]. Acta Materialia. 1996, 44(1): 127−136.

[42] SINGH V, MONDAL C, SARKAR R, BHATTACHARJEE P P, GHOSAL P. Dynamic recrystallization of a β(B2)-stabilized γ-TiAl based Ti−45Al−8Nb−2Cr−0.2B alloy: The contributions of constituent phases and Zener−Hollomon parameter modulated recrystallization mechanisms [J]. Journal of Alloys and Compounds, 2020, 828: 154386.

[43] LI Lian, LI Miao-quan. Constitutive model and optimal processing parameters of TC17 alloy with a transformed microstructure via kinetic analysis and processing maps [J]. Materials Science and Engineering A, 2017, 698: 302−312.

[44] CHAO H Y, SUN H F, CHEN W Z, WANG E D. Static recrystallization kinetics of a heavily cold drawn AZ31 magnesium alloy under annealing treatment [J]. Materials Characterization, 2011, 62(3): 312−320.

[45] KAZEMINEZHAD M. On the modeling of the static recrystallization considering the initial grain size effects [J]. Materials Science and Engineering A, 2008, 486: 202−207.

[46] LAASRAOUI A, JONAS J J. Recrystallization of austenite after deformation at high temperatures and strain rates-analysis and modeling [J]. Metallurgical Transaction A, 1991, 22: 151−160.

网篮组织 TC17 合金的球化定量分析和建模

庞昊宇，罗 皎，张志刚，韩文超，许铿烽，李淼泉

西北工业大学 凝固技术国家重点实验室，西安 710072

摘 要：研究具有网篮组织 TC17 合金的球化行为和机理，建立动态和静态球化的动力学模型。定量和金相结果表明：α 相的球化对变形和热处理工艺参数十分敏感。通过 EBSD 分析，α 内晶界的形成和演化机制与不连续动态再结晶和连续动态再结晶两种机制有关，并在热处理后分别形成和相邻晶粒取向差大和取向差小的两种α晶粒。基于球化行为和机理，建立两种修正 JAMK 模型，分别用于预测动态和静态球化动力学。10.67%和 13.80%的平均相对误差绝对值(MARE)表明动态和静态球化动力学模型的准确性。研究结果可以为钛合金的显微组织调控提供指导。

关键词：TC17 合金；网篮组织；球化；定量分析；动力学模型

(Edited by Bing YANG)